Single exponential decay waveform; a synergistic combination of electroporation and electrolysis (E2) for tissue ablation

Nina Klein Corresp., 1, 2 , **Enric Guenther** 1, 2 , **Paul Mikus** 1 , **Michael K Stehling** 1, 2 , **Boris Rubinsky** 1, 3

1 Inter Science GmbH, Gisikon, Switzerland

2 Prostata Center, Institut fur Bildgebende Diagnostik, Offenbach, Germany

3 Department of Mechanical Engineering, University of California, Berkeley, Berkeley, United States

Corresponding Author: Nina Klein
Email address: n.klein@biophysik.org

Background: Electrolytic ablation and electroporation based ablation are minimally invasive, non-thermal surgical technologies that employ electrical currents and electric fields to ablate undesirable cells in a volume of tissue. In this study we explore the attributes of a new tissue ablation technology that simultaneously delivers a synergistic combination of electroporation and electrolysis (E2).

Method: A new device that delivers a controlled dose of electroporation field and electrolysis currents in the form of a single exponential decay waveform (EDW), was applied to the pig liver and the effect of various parameters on the extent of tissue ablation was examined with histology.

Results: Histological analysis shows that E2 delivered as EDW can produce tissue ablation in volumes of clinical significance, using electrical and temporal parameters which, if used in electroporation or electrolysis separately, cannot ablate the tissue

Discussion: The E2 combination has advantages over the three basic technologies of non-thermal ablation: electrolytic ablation, electrochemical ablation (reversible electroporation with injection of drugs) and irreversible electroporation. E2 ablates clinically relevant volumes of tissue in a shorter period of time than electrolysis and electroporation, without the need to inject drugs as in reversible electroporation or use paralyzing anesthesia as in irreversible electroporation.

1 **Single exponential decay waveform; a synergistic combination of**
2 **electroporation and electrolysis (E2) for tissue ablation**

4 Nina Klein[1,2*], Enric Gunther[1,2*], Paul Mikus[1], Michael Stehling[1,2], Boris Rubinsky[1,3]
5
6 [1]Inter Science GmbH, Biophysics, 6038 Gisikon, Luzern, Switzerland
7 [2]Institut fur bildgebende Diagnostik, Prostata Center, 63067 Offenbach, Germany
8 [3]Department of Mechanical Engineering, University of California Berkeley, Berkeley CA 84720
9 USA
10
11 Corresponding Author: Nina Klein
12
13 E-mail address – n.klein@biophysik.org
14

16 **Abstract**

17 Background: Electrolytic ablation and electroporation based ablation are minimally invasive, non-
18 thermal surgical technologies that employ electrical currents and electric fields to ablate
19 undesirable cells in a volume of tissue. In this study we explore the attributes of a new tissue
20 ablation technology that simultaneously delivers a synergistic combination of electroporation
21 and electrolysis (E2).
22 Method: A new device that delivers a controlled dose of electroporation field and electrolysis
23 currents in the form of a single exponential decay waveform (EDW), was applied to the pig liver
24 and the effect of various parameters on the extent of tissue ablation was examined with
25 histology.
26 Results: Histological analysis shows that E2 delivered as EDW can produce tissue ablation in
27 volumes of clinical significance, using electrical and temporal parameters which, if used in
28 electroporation or electrolysis separately, cannot ablate the tissue
29 Discussion: The E2 combination has advantages over the three basic technologies of non-thermal
30 ablation: electrolytic ablation, electrochemical ablation (reversible electroporation with injection
31 of drugs) and irreversible electroporation. E2 ablates clinically relevant volumes of tissue in a
32 shorter period of time than electrolysis and electroporation, without the need to inject drugs as
33 in reversible electroporation or use paralyzing anesthesia as in irreversible electroporation.
34

35 **Keywords**
36 tissue   ablation,   liver,   electrolytic   ablation,   reversible   electroporation,   irreversible
37 electroporation, synergy electroporation and electrolysis
38
39
40

Introduction

A number of biophysical and biochemical phenomena occur simultaneously when electrical potentials are applied across biological matter. These include Joule heating due to electrical current energy dissipation, electrolytic reactions at the interface between the electrodes and the biological milieu, and cell membrane permeabilization known as electroporation. All these electrical phenomena are used for tissue ablation. Usually the electrical potential delivery protocol is designed in such a way as to maximize one phenomenon, while minimizing the others. For example, in non-thermal irreversible electroporation (NTIRE) the electrical potential profile is designed to maximize irreversible electroporation while minimizing Joule heating (Davalos et al. 2005). The non-thermal aspect of NTIRE was found to be beneficial in tissue ablation treatments, in which it is desired to spare vital sites in the treated lesion, such as blood vessels and nerves.

In electrolytic tissue ablation, cell death is caused by the chemical interaction between the products of electrolysis and cells (Nilsson et al. 2000),(Czymek et al. 2011). Because the ablation is caused by a chemical reaction, it is a function of compounds concentration and time of exposure. One drawback of tissue ablation by electrolysis is the need for high concentrations of electrolytes and lengthy times of exposure. An advantage is the very low currents and voltages used.

In ablation by electroporation, brief, pulsed, high electric fields are used to permeabilize the cell membrane. Lower electric fields and small numbers of pulses yield reversible electroporation, in which the cell membrane permeabilization is temporary. Higher electric fields with larger number of pulses yield irreversible electroporation in which the cell membrane permeabilization is permanent, which results in cell death. Both reversible and irreversible electroporation are used for tissue ablation, each with their advantages and disadvantages. Reversible tissue electroporation is used for tissue ablation in combination with cytotoxic additives, in a procedure known as electrochemotherapy (Mir et al. 1991), (Marty et al. 2006). One advantage of ablation by means of irreversible electroporation over electrochemotherapy is that no chemotoxic drugs are injected into the tissue (Rubinsky et al. 2007), while the advantage of electrochemotherapy over irreversible electroporation is the use of fewer pulses and lower electric fields. The need to inject cytotoxic additives adds a complicating step to the electrochemotherapy procedure. Cell death through electrochemotherapy is dependent on mitosis cycle rendering and is possibly more tissue selective, while irreversible electroporation induces apoptosis and necrosis instantaneously over the whole volume exposed to sufficiently high fields. However, the high electric fields and the large number of pulses used in conventional irreversible electroporation protocols cause some undesirable effects. They induce muscle contractions that require the use of a muscle relaxant and deep anesthesia during surgery. It should be noticed that in clinical practice, reversible electroporation is mostly used without muscle relaxants and with topical anesthesia (Marty et al. 2006). Every clinical electroporation protocols, reversible or irreversible, generates some products of electrolysis, and some heat. We have recently shown that if substantial amounts of products of electrolysis are inadvertently generated during an

84 electroporation protocol, a highly detrimental electrical discharge across the layer of gas formed
85 on the electrodes can occur (Guenther et al. 2015).
86
87 In several recent papers we have shown that combining electroporation and electrolysis (E2)
88 sagaciously yields a new technology of tissue ablation with certain advantages over tissue
89 ablation by electroporation (reversible or irreversible) or electrolysis alone (Phillips, Raju et al.
90 2015) (Phillips et al. 2016) (Stehling et al. 2016). We have developed several possible synergistic
91 electroporation and electrolysis (E2) protocols. One effective combination entails delivering first
92 several (eight) reversible electroporation type pulses followed by the injection of a low voltage
93 direct current to generate products of electrolysis. While effective, this combination requires two
94 different power supplies, one for electroporation and the second for electrolysis (Phillips et al.
95 2015) (Phillips et al. 2016) (Stehling et al. 2016). The combined voltage profile of electroporation
96 pulses followed by low voltage electrolysis reminded us of an exponential decay waveform
97 (EDW), generated by the discharge of a capacitor; a type of pulse which was rather common in
98 the early stages of electroporation research (Sale and Hamilton 1967). The shape of the capacitor
99 discharge exponential decay waveform is a high initial voltage followed by a rapid decay towards
100 a trailing low voltage. This type of waveform is still used in cell electroporation. We thought that
101 with a properly chosen set of capacitor discharge parameters, the initial high voltage over a
102 suitable timeframe could serve for electroporation, while the trailing lower voltage could
103 generate sufficient charge for the generation of electrolytic products. The feasibility of tissue
104 ablation with a EDW, was shown in the liver of a small rodent (Phillips et al. 2016). Here, we
105 extend the study to a large animal model, pig liver, and show that EDW has the ability to ablate
106 tissue volumes of clinical significance. The experimental study was supported by a mathematical
107 analysis to evaluate the electric fields and extent of thermal damage generated by the
108 exponential decay waveform.
109
110
111
112
113 **Materials and methods:**
114
115 Animal protocol:
116
117 The study was approved by Sir José Antonio Rodríguez Correa, Director of Animal Health
118 Programs and General Director of Department of Agriculture and Livestock, Ministry of
119 Environment and Rural, Agricultural Policies and Territory, Government of Autonomous
120 Community of Extremadura (Spain), with application form number: 2015209030009567 and
121 study register number: 100370001499. The experiment was conducted on *in vivo* pig liver, which
122 was in accordance with Royal Decree Law 53/2013 (Feb.1st). According to the study protocol,
123 three female pigs between 90-110 kg were treated. After being fasted for 24 hours, animals were
124 pre-medicated with a combination of diazepam (0.4mg/kg) and ketamine (15mg/kg) injected
125 intramuscularly (IM). Anesthesia was induced with intravenous (IV) Propofol (3mg/kg).
126 Endotracheal intubation was performed and anesthesia was maintained with sevoflurane in
127 oxygen (adjusted to 1.8-2% End tidal sevoflurane). Possible postoperative pain was treated with

128   Buprenorphine 0.01 mg/kg IM Pre-med at recovery and Carprofen 4 mg/kg at
129   extubation/recovery. Cefazolin 25 mg/kg IV was administrated every 2 hours. If found to be
130   needed during the procedure, the study had the ability to deliver pancuronium (0.1 mg/kg, at a
131   dose of 1 mg/ml) through an IV to reduce muscle contractions during the application of the
132   electrical pulses. The liver was exposed via a midline incision. The treatment was delivered using
133   two 18-gauge Titanium needles (Inter Science GmbH, Ch) with a variable length (1-4 cm exposed
134   treatment length) insulating sheath inserted in the liver. Titanium was chosen, because, unlike
135   steel or aluminum it is chemically inert, and does not introduce toxic metals in tissue, during the
136   electrolysis stage. In addition, Ti is MRI compatible. The 18-gauge variable length electrodes were
137   custom designed for the delivery of both electroporation and electrolytic pulse sequences.
138
139   Two electrodes were inserted in the liver under ultrasound monitoring, in a roughly axial parallel
140   configuration, normal to the liver surface. Ultrasound images were also taken throughout the
141   procedure. Since no apparatus is currently available to produce the exponential decay voltage
142   waveform needed for the SEE procedure conceived by us, we have designed and built a new
143   power supply described in the following device section. The parameters varied in this study were:
144   the initial voltage and the time constants of the exponential voltage waveform. In addition, we
145   varied the number of exponential voltage waveforms delivered. A total of 23 lesions were
146   produced, in three pigs, in separate experiments. Animals were sacrificed at 24 hours. The pigs
147   were euthanized using Euthasol 1 ml/lb IV.
148
149   To fix the liver for microscopic viewing, a Foley catheter was placed into the descending aorta
150   and the hepatic vein was snipped off for drainage of the affluent. The liver was flushed with
151   physiological saline for ten minutes at a hydrostatic pressure of 80 mmHg from a pressurized IV
152   drip. Immediately following saline perfusion, a 10% formalin fixative was perfused in the same
153   way for ten minutes. The liver lobe in which the SEE lesion was made was removed and stored in
154   the same formalin solution. For microscopic analysis, the tissue was bread loafed perpendicular
155   to the capsule surface and parallel to the needle tracts. All cassettes were processed routinely
156   from 10% phosphate buffered formalin to wax blocks. Five micrometer sections were made from
157   each block and stained with Masson's trichromatic stain for histologic examination. The stained
158   samples were examined and analyzed by an independent histology service company and reports
159   were prepared (Narayan Raju, Inc, South San Francisco, CA). The focus of the histology was to
160   verify the extent and nature of tissue ablation with E2. To produce information of practical clinical
161   value, the focus of the analysis was on verifying the ability to produce a continuous lesion
162   between the electrodes.
163
164   **Device**
165
166   We were unable to find a power supply that can produce the waveform parameters, required for
167   an EDW protocol in tissues with the dimensions of the pig liver. Therefore, we designed a power
168   supply that operates in the modality of capacitor discharge electroporation systems (e.g. Gene
169   Pulser Xcell™ Electroporation System, BioRad, Hercules, CA) with an enhanced performance. The
170   conventional type capacitors used were replaced with a 100 microfarad capacitor to provide the
171   charge required for electrolysis. Similar to the Gene Pulser Xcell™, the generator has an output

172   of up to 3kV. Because of the larger capacitors it can generate exponential decay waveforms up
173   to time ranges of hundred milliseconds, depending on tissue conductivity and thereby
174   simultaneously deliver electrolysis and electroporation. The apparatus selects and matches the
175   internal components needed to produce the time constants selected for the specific tissue
176   conductivity of the treatment area. The apparatus is able to produce and deliver the exponential
177   decay voltage profile in the time and voltage range for the specific treatment area.
178
179   **Mathematical Analysis**
180
181   The thermal and electrical field simulations were performed using a finite element solver (Comsol
182   Multiphysics 5.2) for the Laplace equation (electrical field) and Pennes Bioheat equation, in a way
183   identical to that described in (Davalos et al. 2005). The setup was approximated as two parallel
184   titanium cylinders in a large volume of liver tissue with the parameters shown in Table 1. In case
185   of discharging capacitors, the amount of Joules heating in tissue is prescribed by the dissipation
186   of the charge energy, Q, ($Q=C*U_0$). Therefore, specifying only, the initial voltage (U_0) and capacity
187   (C) is sufficient to simulate the experiment. Permanent tissue damage can occur instantaneously
188   due to temperatures above 90°C, but also chronically with temperatures above 45°C over a
189   period of time depending on cell type and temperature. The latter mechanism is the only effect
190   for pulse-based treatments in the energy magnitude discussed here where distances of more
191   than a millimeter from the electrode could take thermal damage. Therefore, all temperature
192   graphs in the figures show the temperature after 30 seconds of heat dissipation. The waveform
193   delivered to the electrodes was assumed to be a perfect exponential decay in time, t, ($U= U_0*exp$-
194   (t/τ)), where U_0 is the initial voltage and the time constant is, τ. The time constant was taken
195   from the experimental data, through the analysis of the voltage trace during the delivery of the
196   waveform.
197
198
199   **Results**
200
201   A series of 23 lesions were generated in experiments in which we studied the effects of the E2
202   waveform parameters on tissue ablation. The study examined the effects of the initial voltage,
203   the time constant and the number of exponential decay voltage waveforms delivered. To
204   facilitate a systematic and well defined analysis of the E2 phenomenon, we will focus on the
205   results at midline between the two electrodes.
206
207   Figure 1 shows results from a series of studies in which the initial voltage between electrodes
208   was 750 V, the distance between electrodes was 15 mm, the exposed length was 10 mm and the
209   depth of penetration was 20 mm. This configuration produces an initial voltage over distance of
210   500 V/cm. The calculated electrical field norm is displayed in panel A and the calculated
211   temperature in panel B. Geometrically, both graphs represent the 1d-cutline through the
212   perpendicularly induced electrodes with the electrical field and the temperatures respectively on
213   the y-axis. Panels C and D are the macroscopic histology from lesions treated with a voltage
214   difference of 750 V between the electrodes and time constants of 50 ms and 100 ms, respectively.
215   If tissue resistance and conduction between electrode and tissue were constant, the discharge

216 could be fully described using the time constant of the EDW. However, secondary effects like thin
217 layers of burned tissue, can cause insulation and hence disrupt the ideal exponential decay. This
218 does not necessarily have any negative effect on the ablation, but will limit τ to adequately
219 describe the delivered waveform. The panels show the formalin embedded samples, sectioned
220 in a plane that is transverse to the centers of the two electrodes. In all the different experiments
221 with 750 V (500 V/cm voltage to distance between electrodes) there was no configuration in
222 which the lesion between electrodes became continuous. Panels A and B show that at the line
223 midway between the electrodes the electric field is less than 200 V/cm and the temperature is
224 below 40°C.

226   Figure 2 shows results from an experiment in which the initial voltage between electrodes was
227 1000 V, the distance between electrodes was 15 mm, the exposed length was 10 mm, the depth
228 of penetration was 20 mm and the time constant was 70 ms. The slides were prepared with
229 Masson's trichrome staining. Fig A gives an overview of the evaluated slide. The image is taken
230 in a plane that transverses the centers of the two electrodes. The area of the probe is clearly
231 visible, with a deep blue color at the site of the probes, representing the cellular damage caused
232 by thermal necrosis, surrounded by areas of coagulated blood (deep red color). 10x magnification
233 at the anode (Fig 2B) illustrates an area of thermal necrosis, where the hepatocytes have
234 sustained more intense cellular ablation injury resulting in denaturation of the cytoplasmic
235 organelles. At the cathode (Fig 2D) we can witness the gradual effect of the treatment: Around
236 the macroscopically visible lesion there is a pale area which represents less affected cells
237 immediately adjacent to the severely affected hepatocytes (marked with an arrow). The
238 sinusoidal spaces are dilated due to edema and/or hepatocellular swelling, while the nuclei are
239 condensed. The space between the electrodes is not fully ablated, as the microscopic images
240 show areas of unaffected cells (Figure 2C). Figure 2E shows the calculated electric field for a
241 voltage of 1000 V and figure 2F shows the calculated temperature distribution. Panels 2E and 2F
242 show that, for these experimental conditions, the minimal electric field midway between the
243 electrodes is calculated to be about 240 V/cm and the temperature midway between the
244 electrodes is well below 40°C.

246 Figure 3 illustrates the pathology of liver, from a treatment in which two voltage exponential
247 decay waveforms with similar parameters as those that produced Figure 2, were delivered at an
248 interval of 30 seconds. The macroscopic image taken from a plane between the center of the two
249 electrodes (Fig. 3A) shows that the partial electrode pathway (tunnel) is filled with coagulated
250 blood. This is confirmed by the deep red linear region in the histological slides stained with
251 Masson's trichrome staining in Figure 3B to 3D. The dark blue zone around that region (Figs 3B-
252 3D) represents the more severely ablated hepatocytes, by virtue of being closest to the point of
253 energy release. Figure 3E shows the calculated electric field for an exponential decay waveform
254 with an initial voltage of 1000 V and figure 3F shows the calculated temperature distribution at
255 the onset of the second pulse. There are two aspects to notice in panels 3E and 3F. Figure 3E is a
256 copy of Figure 2E. It is obvious because we have used the electrical parameters of normal liver.
257 However, it is known that the electrical conductivity of electroporated tissue changes after
258 electroporation (Ivorra and Rubinsky 2007), and therefore this panel may not be correct. The
259 second aspect relates to the temperature distribution. Figure 3E shows that the calculated

260 temperature distribution, when the second pulse is delivered is substantially elevated over the
261 initial temperature when the first pulse is delivered, and thermal damage may be induced near
262 the electrodes.
263
264 Figure 4 shows 10x magnified images of the histological slide from Figure 3. Fig. 4A shows the
265 space between the electrodes. Fig. 3B gives a 10x magnification of that area, showing a full
266 ablation zone, with affected cells throughout the area. Hepatocytes both at the cathode (Fig 4C)
267 and anode (Fig 4D) show condensed nuclei, with hemorrhage in the spaces between, however
268 with intact vessels (Fig 4C).
269
270 Figure 5 shows the histological results of exponential voltage profile in which the initial voltage
271 between electrodes was 1500 V, the distance between electrodes was 15 mm, the exposed
272 length was 20 mm and the depth of penetration was 30 mm. It is important to notice that the
273 top 10 mm of the electrode was insulated. The slides were prepared with Masson's trichrome
274 staining. Fig 5A shows the cells on the center line between the electrodes at the level of the top
275 10 mm insulated part of the electrodes. Here we see that the cells are not affected by the
276 treatment. The next panel (Fig. 5B), however, shows the lesion which was caused by the
277 treatment in the uninsulated part of the tissue between the electrodes. The lesion is continuous
278 between electrodes at this level. Figure 5C displays the calculated electric field for a voltage of
279 1500 V, and figure 5D shows the calculated temperature distribution. The electric field midway
280 between the electrodes is about 550 V/cm. The midway between electrodes temperature is
281 about 40°C.
282
283 Figure 6 displays a 10x magnification of the pathological slide shown in Figure 5. Panel 6 A is a
284 magnification of the cathode, showing swollen and necrotic hepatocytes and a disrupted
285 sinusoidal pattern. Between the electrodes (Fig. 6B) a bridged ablation with affected cells was
286 observed, with a complete loss of cellular structure. At the anode (Fig. 6C) there is an affected
287 cellular architecture with hemorrhage. Panels 6A-C show open and undamaged large blood
288 vessels within the treatment field.
289
290 A very important observation is that there was no need for muscle paralysis in any of the 23
291 lesions produced with various E2 protocols. This evaluation is based on the assessment of a
292 physician (MS) with an experience of close to 450 NTIRE procedures in which muscle contraction
293 can occur even with deep muscle relaxations.
294
295 **Discussion**
296
297 Our experiment was designed to be performed without a muscle relaxant, however, in such a
298 way as to allow for an immediate use of a muscle relaxant as soon as an undesirable level of
299 muscle contraction is noted. From among the 23 experiments with the exponential decay voltage
300 waveform done in this pig liver study, a muscle contraction requiring the use of a muscle relaxant
301 (pancuronium) was detected in none. In fact, the muscle contraction was negligible, and at times
302 unnoticeable. The E2 treatment was delivered by a physician with an experience of close to 400
303 irreversible electroporation treatments (MS). It was noted that the observed response is clinically

304 acceptable and the exponential decay voltage waveform procedure can be carried out without
305 the use of muscle paralyzing drugs. Obviously this observation is relevant only to the parameters
306 used in this study, in which the maximal voltage was 1500 V (1000 V/cm voltage over distance)
307 and the maximal time constant 148 ms.

308

309 The E2 protocol requires a special waveform comprised of an exponential decay shape with a
310 steep decrease in voltage to values that will not induce an electrical discharge across the
311 electrolytically product near the electrodes and a longer low voltage tail, that can generate
312 sufficient products of electrolysis for the E2 ablation. To the best of our knowledge currently
313 available electroporation systems cannot deliver exponential decay waveforms with the desired,
314 electrolytic products generating time constants. To this end we have modified existing
315 commercial designs (e.g. Gene Pulser Xcell™ Electroporation System, BioRad, Hercules, CA), as
316 described in the methods and materials section. The key difference is the use of larger
317 capacitance, in essentially the same circuit.

318

319 Our main criteria for evaluating the exponential decay voltage waveform ability to ablate tissue
320 in a clinically significant manner was the ability to induce the ablation throughout the gap
321 between the electrodes. Therefore, the histological and mathematical analysis is focused on the
322 tissue found midway between the electrodes. This is the part of the treated tissue in which the
323 lowest electric fields and lowest temperatures occur. Figures 1 and 2 show that there are
324 parameters of initial voltage and time constant for which the tissue midway between the
325 electrodes is not ablated. Figure 1A shows that for an initial voltage of 750 V and a distance of
326 1.5 cm between the electrodes (500 V/cm distance between electrodes), the electric field
327 strength midway between the electrodes is lower than 200 V/cm. This value is substantially
328 below the reversible electroporation threshold for the rabbit liver, which was measured to be
329 362 +/21 V/cm (Miklavcic et al. 2000). Since the calculated temperature midway between
330 electrodes is below 40°C, there is no mechanism to induce damage between the electrodes. The
331 conditions in the region between the electrodes are below the levels required for irreversible
332 electroporation ablation, reversible electroporation or thermal ablation.

333

334 Figure 2 shows that increasing the initial voltage of the exponential decay waveform to 1000 V
335 will also increase the extent of the damage near the electrodes. The distance between the
336 electrodes is 1.5 cm and therefore the initial voltage to distance ratio is 750 V/cm. Figure 2E
337 shows that the electric field midway between electrodes is calculated to be below 300 V/cm. This
338 value is below the 362 +/- 21 V/cm reversible electroporation threshold (Miklavcic et al. 2000).
339 Tissue damage by heat can be also excluded, since the temperature between electrodes does not
340 exceed 40°C (Figure 1B and 2F). In this case also, the conditions in the middle between the
341 electrodes are below the levels required for irreversible electroporation ablation, reversible
342 electroporation or thermal ablation.

343

344 Figures 3 and 4 show that it is possible to ablate the entire zone between electrodes by using two
345 consecutively delivered exponential decay waveforms with the same parameters as those used
346 to produce the results in Figure 2. The initial voltage of the exponential decay waveform was
347 1000 V. The distance between the electrodes is 1.5 cm and therefore, the initial voltage to

348   distance ratio is 750 V/cm. The mechanism of ablation may be related to the possibility that the
349   second exponential waveform has brought the tissue midway between electrodes to the
350   threshold of E2 ablation. Figure 3F shows that the temperature prior to the delivery of the second
351   exponential waveform is elevated relative to that prior to the delivery of the first waveform.
352   Elevated temperatures favor electroporation and may reduce its threshold. Furthermore, it is
353   known that electroporation changes the electrical conductivity of tissue. While Figure 3E was
354   obtained for the electrical conductivity of the normal liver, the second waveform may generate
355   a somewhat modified electric fields. Last, the second waveform has delivered twice the level of
356   electrolytic compounds than in the experiment whose results are depicted in Figure 2. This
357   tentatively suggests that the mechanism of tissue ablation in the middle part of the tissue
358   between electrodes is the synergy between reversible electroporation and electrolysis.
359
360   The results displayed in Figures 5 and 6 produce stronger evidence of the E2 mechanism of tissue
361   ablation. Here, an increase of the exponential decay waveform initial voltage to 1500 V has
362   produce ablated tissue between the electrodes. Calculations show that the electric field midway
363   between the electrodes is about 550 V/cm (Figure 5E). This value is below the irreversible
364   electroporation threshold for the rat liver (637 V/cm +/- 43 V/cm)(Miklavcic et al. 2000). The
365   temperature midway between electrodes is about 40°C, (Figure 5F), which is below the threshold
366   of thermal damage. The mechanism of tissue ablation at the midpoint between electrodes is
367   neither irreversible electroporation nor thermal. The most likely possible mechanism is the
368   synergistic effect of electrolysis and reversible electroporation.
369
370   This is a first large animal study on the use of the synergy between electrolysis and reversible
371   electroporation to enhance tissue ablation by electroporation. However, the E2 combination
372   seems promising. It has the ability to create comparable clinically relevant areas of tissue
373   ablation, in a much shorter period of time than irreversible electroporation, with lower voltages
374   and single waveforms, without the need to inject drugs and without the need for paralyzing
375   anesthesia.
376
377
378

379   **Acknowledgements**
380
381   We would like to thank Dr. Narayan Raju from Pathology Research Laboratory, Inc for his
382   assistance on the pathological examination and analysis.

383
384
385   **Author contributions statement**
386
387   B.R. conceived the experiment, M.S., P.M., E.G., N.K. and B.R. conducted the experiment, E.G.
388   B.R. and N.K. analyzed the results. All authors reviewed the manuscript.
389
390
391

392 **References**

393

394 Czymek, R., D. Dinter, S. Loeffler, M. Gebhard, T. Laubert, A. Lubienski, H.-P. Bruch and A. Schmidt
395 (2011). "Electrochemical Treatment: An Investigation of Dose-Response Relationships Using an
396 Isolated Liver Perfusion Model." Saudi Journal of Gastroenterology **17**(5): 335-342.
397 Davalos, R. V., L. M. Mir and B. Rubinsky (2005). "Tissue ablation with irreversible
398 electroporation." Annals of Biomedical Engineering **33**(2): 223-231.
399 Guenther, E., N. Klein, P. Mikus, M. K. Stehling and B. Rubinsky (2015). "Electrical breakdown in
400 tissue electroporation." Biochemical and Biophysical Research Communications **467**(4): 736-741.
401 Ivorra, A. and B. Rubinsky (2007). "In vivo electrical impedance measurements during and after
402 electroporation of rat liver." Bioelectrochemistry **70**(2): 287-295.
403 Marty, M., G. Sersa, J. R. Garbay, J. Gehl, C. G. Collins, M. Snoj, V. Billard, P. F. Geertsen, J. O.
404 Larkin, D. Miklavcic, I. Pavlovic, S. M. Paulin-Kosir, M. Cemazar, N. Morsli, Z. Rudolf, C. Robert, G.
405 C. O'Sullivan and L. M. Mir (2006). "Electrochemotherapy - An easy, highly effective and safe
406 treatment of cutaneous and subcutaneous metastases: Results of ESOPE (European Standard
407 Operating Procedures of Electrochemotherapy) study." EJC Supplements **4**(11): 3-13.
408 Miklavcic, D., D. Semrov, H. Mekid and L. M. Mir (2000). "In vivo electroporation threshold
409 determination." Proceedings of the 22nd Annual International Conference of the IEEE
410 Engineering in Medicine and Biology Society (Cat. No.00CH37143): 2815-2818 vol.2814.
411 Mir, L. M., M. Belehradek, C. Domenge, S. Orlowski, B. Poddevin, J. J. Belehradek, G. Schwaab, B.
412 Luboinski and C. Paoletti (1991). "Electrochemotherapy, a new antitumor treatment: first clinical
413 trial." Comptes Rendus de l'Academie des Sciences Serie III Sciences de la Vie **313**: 613-618.
414 Nilsson, E., H. von Euler, J. Berendson, A. Thorne, P. Wersall, I. Naslund, A. S. Lagerstedt, K.
415 Narfstrom and J. M. Olsson (2000). "Electrochemical treatment of tumours." Bioelectrochemistry
416 **51**(1): 1-11.
417 Phillips, M., H. Krishnan, N. Raju and B. Rubinsky (2016). "Tissue ablation by a synergistic
418 combination of electroporation and electrolysis delivered by a single pulse." Annals of Biomedical
419 Engineering.
420 Phillips, M., N. Raju, L. Rubinsky and B. Rubinsky (2015). "Modulating electrolytic tissue ablation
421 with reversible electroporation pulses." Technology **3**(1): 45-53.
422 Rubinsky, B., G. Onik and P. Mikus (2007). "Irreversible electroporation: A new ablation modality
423 - Clinical implications." Technology in Cancer Research & Treatment **6**(1): 37-48.
424 Sale, A. J. H. and W. A. Hamilton (1967). "Effects of high electric fields on microorganisms. 1.
425 Killing of bacteria and yeasts." Biochimica et Biophysica Acta **148**: 781-788.
426 Stehling, M. K., E. Guenther, P. Mikus, N. Klein, L. Rubinsky and B. Rubinsky (2016). "Synergistic
427 Combination of Electrolysis and Electroporation for Tissue Ablation." Plos One **11**(2).

428

429

Initial Voltage U_0	750V (Fig.2), 1000V (Fig.3,4), 1500V (Fig.5)
Exposure length	1cm (Fig.2,3,4) 2cm (Fig.5)
Decay	Exponential capacitor discharge
Power supply capacitance	Listed in Figures
Distance between electrodes	1.5cm
Electrode diameter	1mm
Liver: electrical conductivity	0.286 S/m
Liver: heat capacity	3750 J/(kg*K)
Liver: density	1000 kg/m^3
Liver: thermal conductivity	0.52 W/(m*K)
Titanium: electrical conductivity	7.4e5 S/m
Titanium: heat capacity	710 J/(kg*K)
Titanium: density	4940 kg/m^3
Titanium: thermal conductivity k	7.5 W/(m*K)

430

431 Table 1: Parameters used for the thermal and electrical field calculations.

432

433
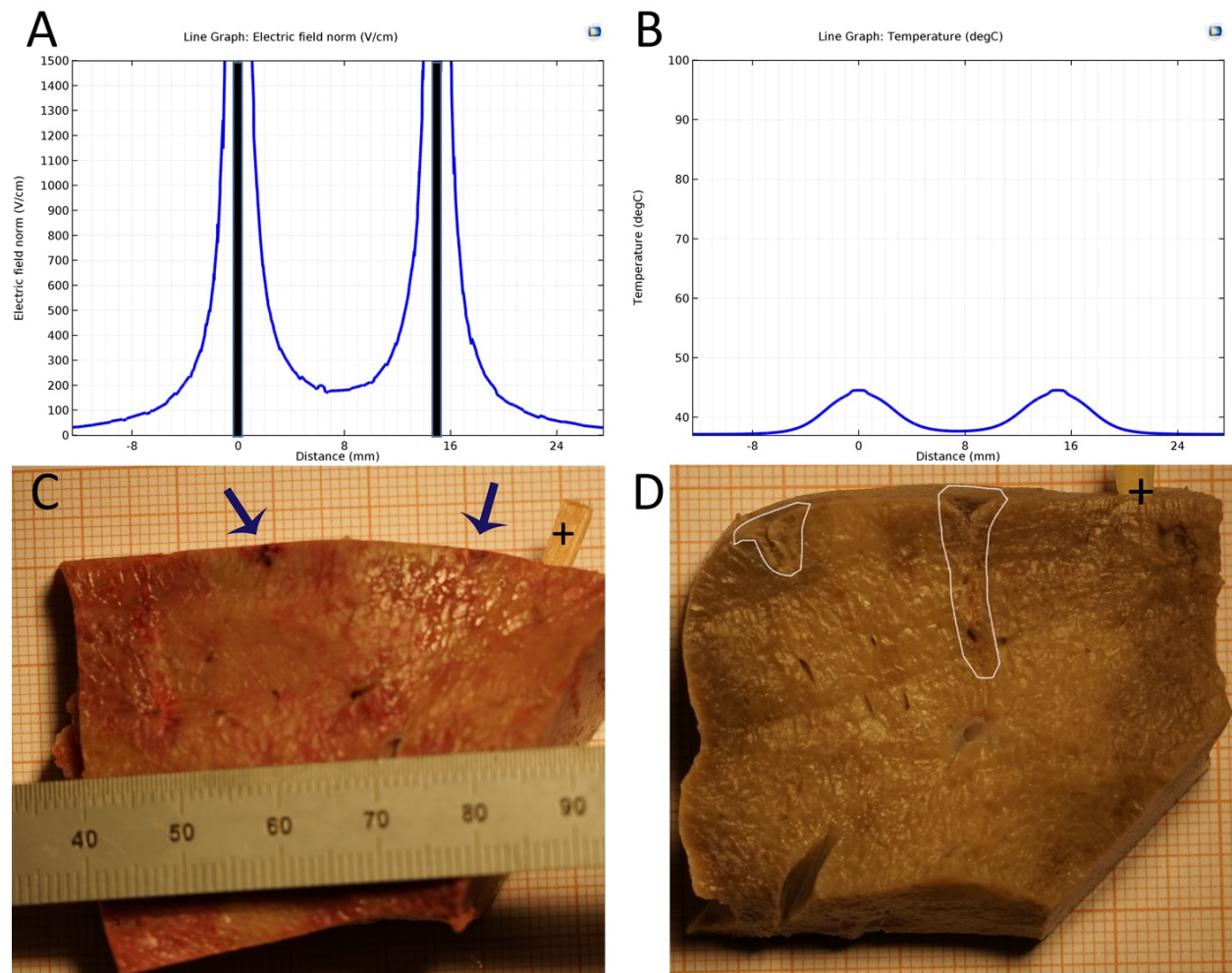
434
435
436 **Figure 1:** Study with an EDW with initial voltage difference between electrodes of 750 V and various time
437 constants. **A.** calculated electric field. **B.** Calculated thermal field after 30 seconds. **C.** Macroscopic image
438 - 50 ms time constant – no ablation was noticed. **D.** Macroscopic image - 100 ms time constant – some
439 ablation near electrodes.
440
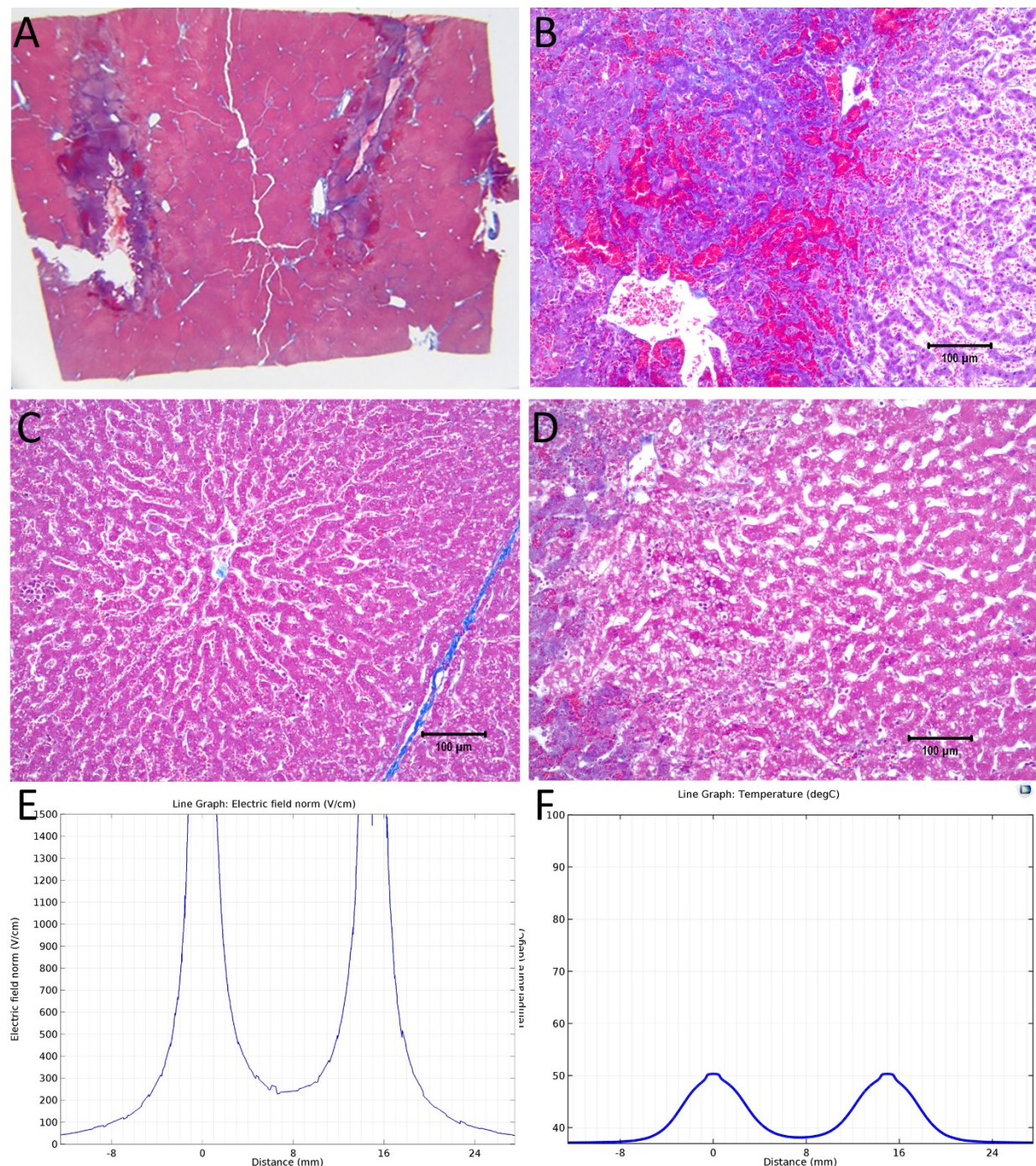
441
442
443 **Figure 2:** Study with one EDW with initial voltage difference between electrodes of 1000 V and time
444 constant of 70 ms. **A.** Histological slide with Masson's trichrome staining. **B.** 10x magnification of the right
445 lesion, which is the anode. We see severe acute hepatocellular necrosis with coagulated blood
446 (hemorrhage) in the sinusoids. **C.** 10x magnification between the electrodes. The cells do not appear to
447 be affected. **D.** 10x magnification at the margin of the left lesion, which is the cathode. Here we see the
448 borderline between the necrotic tissue on the left and partially affected cells on the right. **E.** Electric field
449 strength distribution. **F.** Temperature distribution after 30 seconds. (scale bar 100 μm)
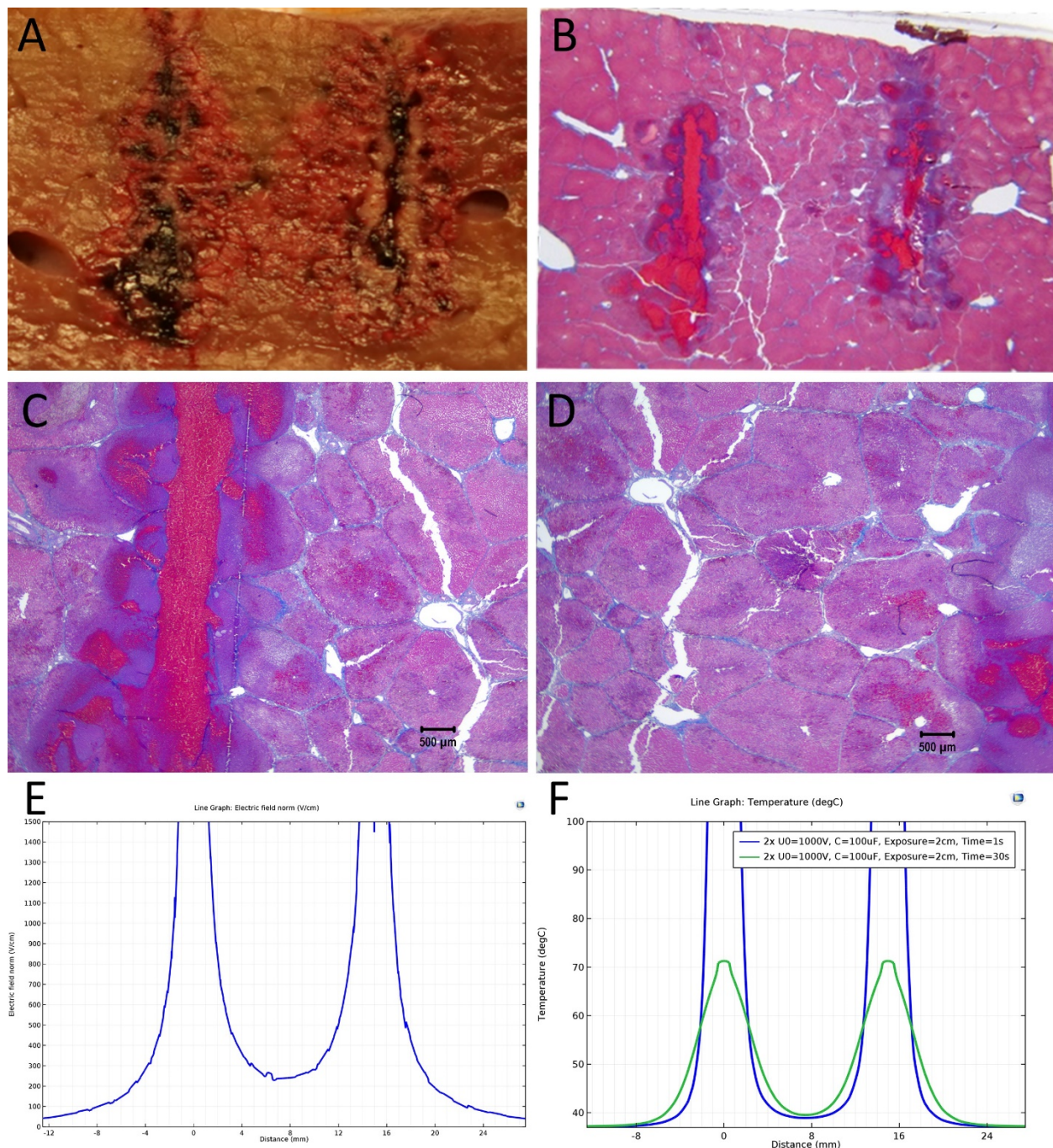
450
451
452 **Figure 3:** Study with 2 EDW separated by 30 s with time constants of 79 and 92 ms, the first and second
453 pulse respectively, 1000 V difference between electrodes placed at a distance of 15 mm between them,
454 10 mm exposed length, 100 µF capacitor. Liver was extracted 18.5 h after treatment. **A.** Macroscopic
455 histological slide (cathode left electrode anode right electrode) **B.** Masson's trichrome staining reveals
456 blood coagulation (red) and ablation both around and in between electrodes. **C.** Close-up of the cathode,
457 which is the left electrode. **D.** Close-up of the right electrode, which is the anode. (scale bar 500 µm) **E.**
458 Electric field strength distribution. **F.** Temperature distribution prior to the delivery of the second
459 waveform at 1 and 30 seconds.
460
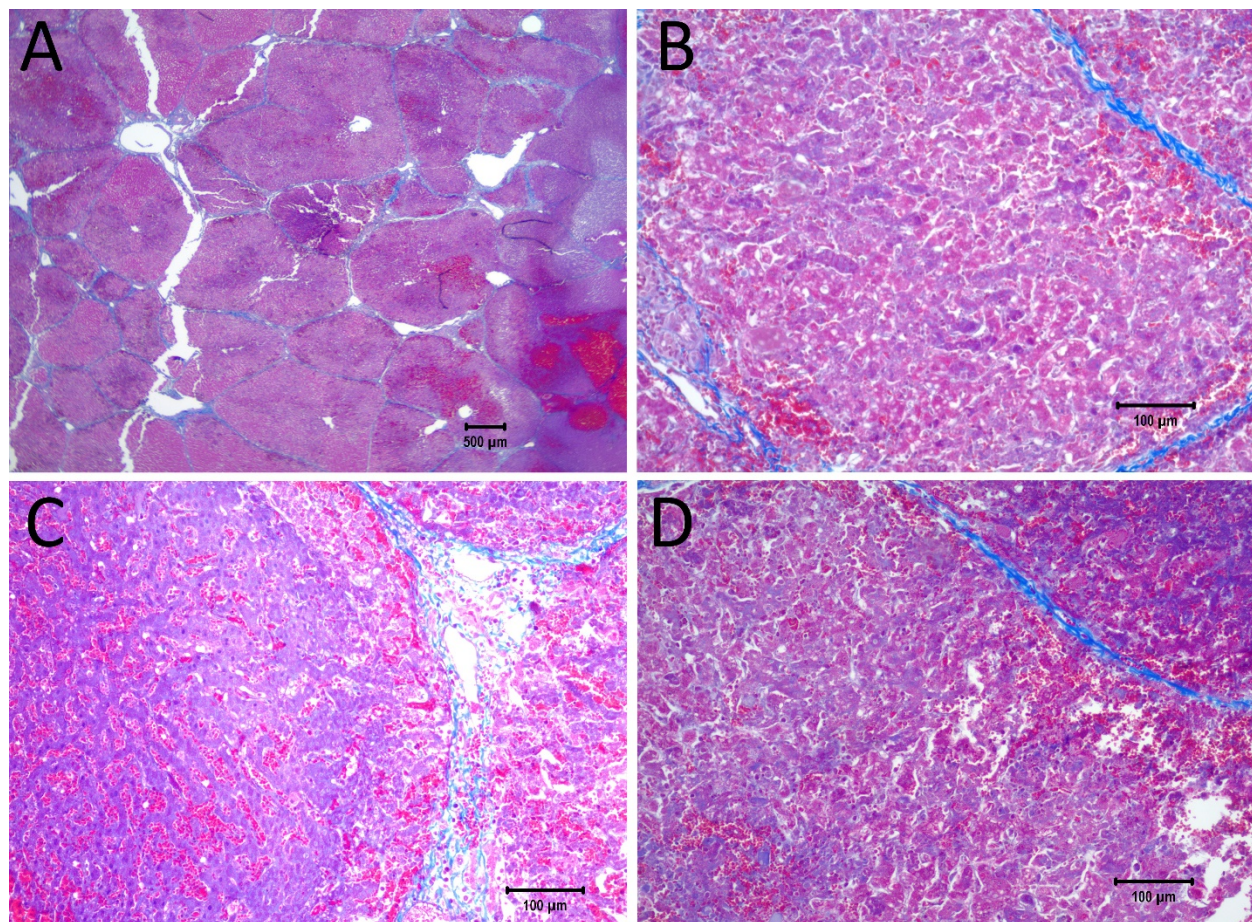
461
462
Figure 4: Details from Figure 3. **A.** Space between the electrodes in Figure 3. Bar indicates 500 µm. **B.** 10x
magnification of cells between the electrodes, showing the details of the ablated area. **C.** 10x
magnification of the cathode, showing edema and cellular ablation injury. **D.** 10x magnification of the area
by the anode, showing the margin of affected and non-affected cells. All images show Masson's trichrome
staining. Bars in B-D indicate 100 µm.
468
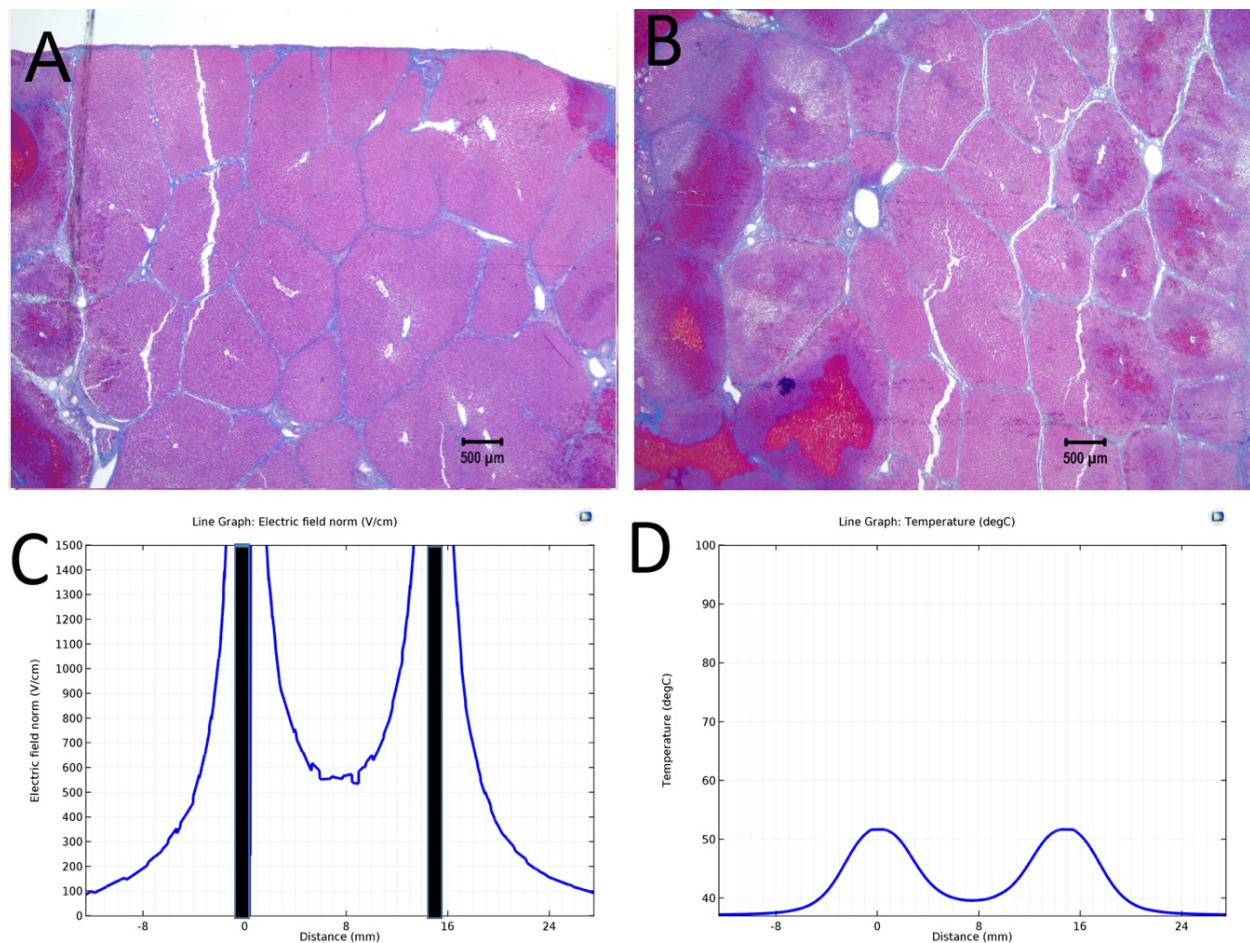
469
470
471 **Figure 5:** Study with a EDW with a time constant of 69 ms, 1500 V difference between electrodes placed
472 at a distance of 15 mm between them, 200 mm exposed length, 100 µF capacitor. **A.** Macroscopic cross
473 section in a plane through the axis of the electrodes. Image taken between electrodes at the part where
474 the electrodes were insulated, showing that the cells are not affected. **B.** Image taken between electrodes
475 where the electrodes were not insulated showing that the lesion was bridged. (500 µm bar). **C.** Electric
476 field strength distribution. **D.** Temperature distribution after 30 seconds.
477
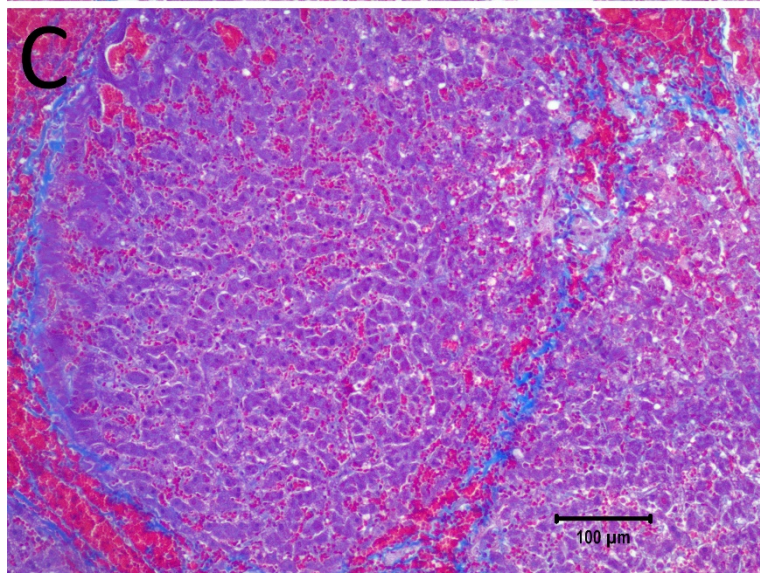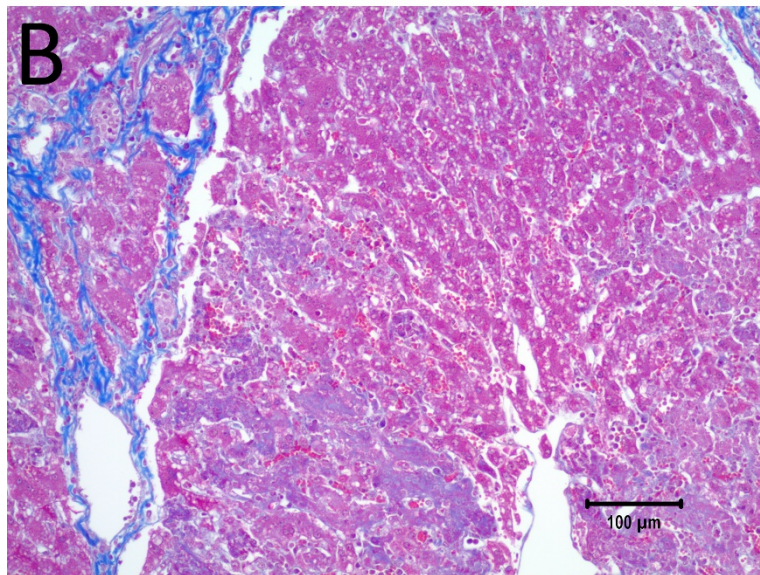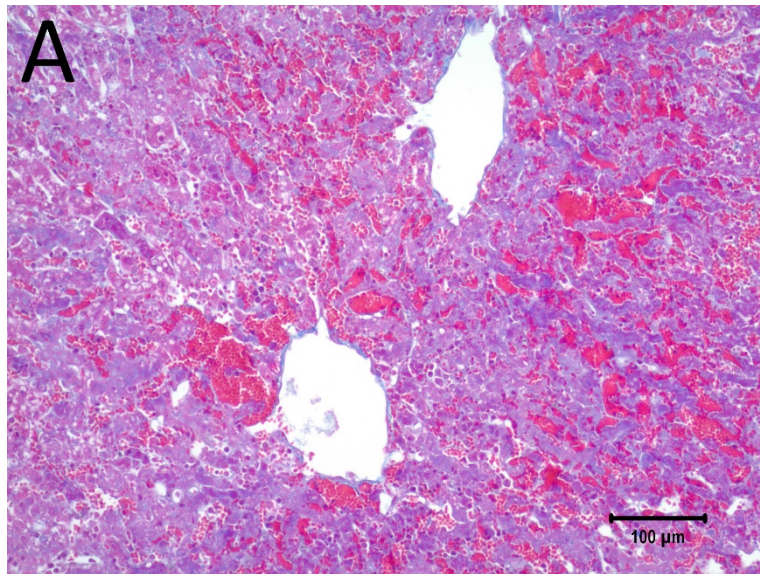
479
480 **Figure 6:** 10x magnification of the pathological slides shown in Fig 5. **A.** Image taken at the right
481 electrode, which was the cathode, showing necrotic, swollen hepatocytes and a disrupted sinusoidal
482 pattern. **B.** Image taken between the electrodes, illustrating a complete loss of cellular structure with
483 swollen hepatocytes. **C.** Left electrode, which was the anode, showing an affected cellular architecture
484 and hemorrhage. Note that the large blood vessels are open and unaffected. Scale bar 100 μm
485